Effects of Self-Assembled Monolayer Modification of Nickel Oxide Nanoparticles Layer on the Performance and Application of Inverted Perovskite Solar Cells

Qin Wang,[a, c] Chu-Chen Chueh,[a] Ting Zhao,[a] Jiaqi Cheng,[d] Morteza Eslamian,*[c] Wallace C. H. Choy,[d] and Alex K.-Y. Jen*[a, b]

Entirely low-temperature solution-processed ($\leq 100\,^\circ$C) planar p-i-n perovskite solar cells (PSCs) offer great potential for commercialization of roll-to-roll fabricated photovoltaic devices. However, the stable inorganic hole-transporting layer (HTL) in PSCs is usually processed at high temperature (200–500 $^\circ$C), which is far beyond the tolerant temperature ($\leq 150\,^\circ$C) of roll-to-roll fabrication. In this context, inorganic NiO$_x$ nanoparticles (NPs) are an excellent candidate to serve as the HTL in PSCs, owing to their excellent solution processability at room temperature. However, the low-temperature processing condition is usually accompanied with defect formation, which deteriorates the film quality and device efficiency to a large extent. To suppress this setback, we used a series of benzoic acid self-assembled monolayers (SAMs) to passivate the surface defects

of the NiO$_x$ NPs and found that 4-bromobenzoic acid could effectively play the role of the surface passivation. This SAM layer reduces the trap-assisted recombination, minimizes the energy offset between the NiO$_x$ NPs and perovskite, and changes the HTL surface wettability, thus enhancing the perovskite crystallization, resulting in more stable PSCs with enhanced power conversion efficiency (PCE) of 18.4 %, exceeding the control device PCE (15.5 %). Also, we incorporated the above-mentioned SAMs into flexible PSCs (F-PSCs) and achieved one of the highest PCE of 16.2 % on a polyethylene terephthalate (PET) substrate with a remarkable power-per-weight of 26.9 W g^{-1}. This facile interfacial engineering method offers great potential for the large-scale manufacturing and commercialization of PSCs.

Introduction

The intriguing perovskite solar cells (PSCs) have aroused tremendous interest owing to their excellent optoelectronic properties, long charge-carrier lifetime, low-temperature solution processability, and relatively low fabrication cost, with a remarkable certified power conversion efficiency (PCE) of 22.1 %,

which could now compete with the commercialized silicon solar cells, if the device stability can be improved.[1] Generally speaking, the current state-of-the-art PSCs adopt a planar heterojunction architecture that could be fabricated with either n-i-p or p-i-n structure, due to the ambipolar transport property of the perovskite light harvesters.[2] However, the n-i-p type suffers from severe hysteresis setback owing to the unbalanced charge distribution in the perovskite layer.[3] Considering the fact that the electron-diffusion length in perovskites is relatively longer than the hole-diffusion length, the p-i-n structure is more advantageous to obtain a reasonably stable device performance.[4, 5] Employing a suitable hole-transporting layer (HTL) is a prerequisite for developing a high-performance p-i-n PSC, because the HTL not only facilitates effective hole collection but also minimizes the interfacial charge recombination.[6]

The most frequently used HTL in PSCs is poly(3,4-ethylenedioxythiophene):polystyrene sulfonate (PEDOT:PSS) and nickel oxide (NiO$_x$). Although PEDOT:PSS is a commercialized and standard HTL material, it suffers from several intrinsic problems such as hygroscopicity, acidity-induced instability, and large potential loss due to unmatched energy level with the adjacent layers in the PSC structure.[7] In contrast, p-type NiO$_x$ is advantageous due to its large band gap (3.5–3.9 eV),[8] deep valence band (5.1–5.4 eV),[9–11] high mobility ($\approx 10^{-3}$ cm^{2}V^{-1}s^{-1})[12, 13] induced by the large doping of Ni^{3+} ion,[13] and its superior stability[14] resulting from its inorganic nature, which brings about a longer device lifetime.[15] To date,

[a] Q. Wang, Dr. C.-C. Chueh, T. Zhao, Prof. A. K.-Y. Jen
Department of Materials Science and Engineering
University of Washington
Seattle, WA, 98105 (USA)
E-mail: ajen@uw.edu

[b] Prof. A. K.-Y. Jen
Department of Materials Science & Engineering
City University of Hong Kong
Kowloon, Hong Kong (SAR China)

[c] Q. Wang, Prof. M. Eslamian
University of Michigan-Shanghai Jiao Tong University Joint Institute
Shanghai, 200240 (P. R. China)
E-mail: Morteza.Eslamian@sjtu.edu.cn

[d] J. Cheng, Prof. W. C. H. Choy
Department of Electrical and Electronic Engineering
The University of Hong Kong
Pokfulam, Hong Kong (SAR China)

a variety of processing strategies for the fabrication of NiO$_x$ thin films have been reported, such as sol-gel,[16] sputtering,[12] pulsed laser deposition,[10] spray pyrolysis,[14] electrochemical deposition,[17] and so on. However, most of the current techniques either require high-temperature deposition processes or high-temperature post-treatment, which are not compatible with the roll-to-roll fabrication.[18] Recently, room-temperature solution-processed NiO$_x$ nanoparticles (NPs)[8,11,19–23] have been considered as the building blocks for NiO$_x$ thin films. Choy and co-workers employed nonstoichiometric NiO$_x$ NPs with a cubic rock-salt structure and octahedral Ni^{2+} and O$^{2−}$ sites as the HTL in organic and PSCs.[11,19,20] These room-temperature solution-processed NP-based NiO$_x$ films (in the following context, we use NiO$_x$ to refer to all NP-based NiO$_x$) demonstrated excellent optoelectronic properties, without the need for post-treatment. By changing the preparation method, Yin et al. deposited low-temperature solution-processed NiO$_x$ films on flexible poly(ethylene 2,6-naphthalate) (PEN) substrates and fabricated flexible PSC with a PCE of 13.43%.[22] Hou et al. adopted low-temperature solution-processed NiO$_x$ nanocrystal ink to fabricate PSCs with PCE of 17.5% and achieved a potential loss as low as 0.226 V.[23] Although the PCE of p-i-n type PSCs incorporating NiO$_x$ HTL has surpassed 17%, it is still barely satisfactory compared with the n-i-p type PSCs, owing mainly to their inferior fill factor (FF) and current density.[4] This may be ascribed to the fact that the low-temperature processing of metal oxides usually leaves behind defects in the film structure. Such defects, therefore, result in poor contact between the NiO$_x$ film and the perovskite layer, which not only influences the perovskite crystallinity and morphology but also causes charge recombination and lower light absorption.[9,10,24]

One potential approach to simultaneously tackle the morphology and charge selectivity problems is to use self-assembled monolayers (SAMs),[25–27] which have proved to be an effective way to change the interfacial properties between the charge-transfer layer (CTL) and the perovskite layer.[6,28] Typically, SAMs are thermodynamically favored ordered monolayer-forming modifiers comprising a head group, a spacer, and a tail group. The head group could be anchored to the surface through physisorption or a preferred chemisorption. The spacer group determines separation of the intermolecular in-

teractions, which is usually in the form of aromatic rings or alkane chains.[26] The tail group could be designed to endow various functions through synthetic chemistry, in which such functional groups could in turn remarkably alter the wettability of the upper layer, facilitating the deposition of the forthcoming layer through both dipolar and dispersive interactions,[29] which further influences the crystallinity, morphology, and energy level offset.[25,30,31] Recently, Snaith and Jen and co-workers reported a C$_{60}$-SAM deposited on titanium dioxide (TiO$_2$) that had electronic coupling with the perovskite layer and achieved a significantly reduced device hysteresis.[32] Han and co-workers applied an organic silane SAM to the TiO$_2$–perovskite interface to change the crystallinity and morphology of the perovskite and achieved efficient fully printable PSCs.[33] Zuo et al. adopted C$_3$-SAM[34] and 4-pyridinecarboxylic acid SAM[35] to tailor the energy levels of zinc oxide and tin dioxide thin films, respectively, and observed significant enhancement in the photovoltaic performance. However, most of current works in the PSCs field that have used SAMs to modify the interfacial properties between the CTL and perovskite layer are centered about the electron-transfer layer (ETL) in n-i-p type PSCs. The application of SAMs to modify the HTL has few examples, especially for low-temperature solution-processed NiO$_x$ HTL in p-i-n type PSCs.

Herein, we first systematically investigated the separate role of the chemical interaction between the NP-based NiO$_x$ and perovskite layers by inserting suitable para-substituted benzoic acid (R-BA) SAMs, as depicted in Scheme 1. According to Choy and co-workers,[11,20] the surface functional groups of the NiO$_x$ NPs are the hydroxylated groups, which can react with the carboxyl groups.[9,36] The purpose of using the SAMs with different dipole moments are as follows: i) to serve as a "glue" to improve the adhesion between the NiO$_x$ film and the ionic perovskite layer to better facilitate the charge transfer by passivating inorganic surface trap states;[33,36] ii) to modify the work function (WF) of the NiO$_x$ NPs through their molecular ordering induced by the permanent dipole moments;[27] iii) to change the perovskite crystallinity and morphology through chemical interactions by means of different terminated functional groups.[33,34] The gas-phase dipole moments of the benzoic acid derivatives are increased in sequence when the tail
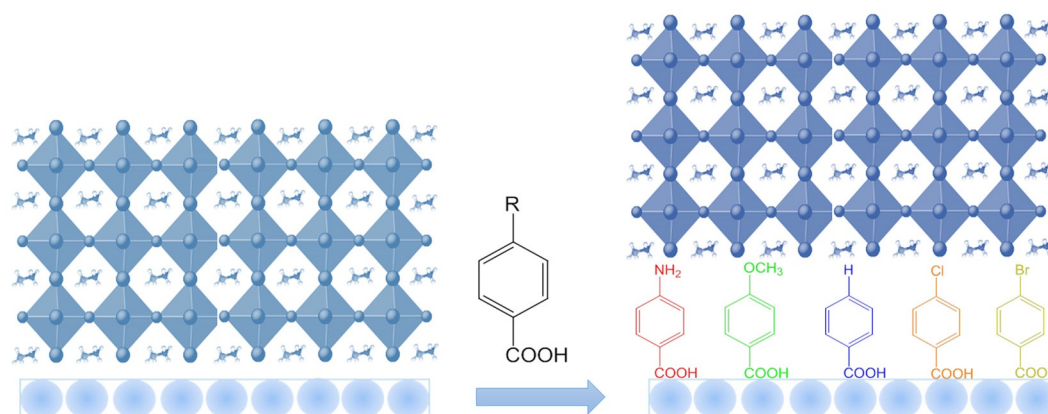
Scheme 1. Schematic diagram of the NiO$_x$/ MAPbI$_3$ structure (left) and NiO$_x$/ SAMs/ MAPbI$_3$ structure.

groups are substituted by $-NH_2$ (-4.5 D) $< -OCH_3$ (-3.9 D) $<$ $-H$ (-2.1 D)[38] $< -Cl$ (2.0 D) $< -Br$ (2.1 D) (1 D $\approx 3.336 \times 10^{-30}$ C m),[27,35,39] in which H-BA shows the van der Waals interaction, whereas others present dipolar interactions.[35] The Br$-$BA modifier was found to have a positive effect that largely enhanced the PCE to 18.4% with increased open-circuit voltage (V_{oc}) of 1.11 V, short-circuit current density (J_{sc}) of 21.7 mA cm^{-2}, and FF of 76.3%. In addition, the device stability was improved owing to the minimization of the energy level offset, reduced surface trap states, increased perovskite crystallinity, and enhanced wetting between NiO$_x$ and perovskite layers, outperforming the control group (PCE of 15.5%) in terms of both the PCE and stability. Moreover, we incorporated the Br-BA SAM into the flexible PSCs (F-PSCs) and achieved one of the highest PCE of 16.2% on the polyethylene terephthalate (PET) substrate with a remarkable power-per-weight (PPW) of 26.9 W g^{-1}. This simple and facile surface modification technique may further pave the way for the scaling up of the PSCs through roll-to-roll manufacturing processes.

Results and Discussion

The fabrication of SAM-modified NiO$_x$ films can be briefly described as follows: NiO$_x$ NPs solution was first spun onto ITO glass and then different SAMs were spun onto the NiO$_x$ films. After a short time of low-temperature annealing, we used ethanol to wash the film surface to remove the remaining SAMs. Scanning electron microscopy (SEM) was used to investigate the effect of depositing R-BA on the morphology of NiO$_x$. As is shown in Figure S1 (Supporting Information), the surface morphology of pristine NiO$_x$ films and SAM-treated NiO$_x$ films did not change much, all showing good coverage with some pinhole-like black dots area. Figure S2 showed that Br-BA has reacted with the hydroxylated functional group of NiO$_x$ through the FTIR spectroscopy.

Then, we explored the morphology evolution and grain-size distribution of methylammonium iodide (MAPbI$_3$) perovskite layer deposited atop different R-BA modified NiO$_x$ films in Figure 1 a, b. By inserting different SAMs with different terminated functional groups, the perovskite morphology and grain size varies to a large extent. For example, the average perovskite grain size (AGZ) of the reference (Ref) group is 140 nm and its morphology shows some pinholes whereas for the NH$_2$-BA-modified NiO$_x$ films, larger pinholes are present and the AGZ increases to 203 nm. In particular, the Br-BA-modified film shows pinhole-free film with an AGZ of 287 nm, which is more than double that of the reference group. This great enhancement may be a result of the terminated functional group of Br changing the surface wetting of NiO$_x$ films, thus contributing to the larger perovskite grain size.[31] Moreover, it may also interact with the MA$^+$ ions to improve the adhesion through hydrogen bonding, which is another reason for the smooth and flawless perovskite film, confirmed by the enlarged SEM images shown in Figure S3.[28]

The crystallinity of the MAPbI$_3$ perovskite films made on different R-BA-modified underlayers was investigated by X-ray diffraction (XRD), as shown in Figure S4, where the characteristic peaks at 13.9°, 28.3°, and 31.8° correspond to the (110), (220), and (310) crystal planes, respectively. The perovskite based on the Br-BA SAM has the most intensive peak in the (110) plane, which manifests the enhanced crystallinity compared with the reference group. The full width at half maximum (FWHM) peaks associated with the (110) plane, illustrated in Figure 1 c, are a more vivid way to further elucidate the dislocation or vacancies in the MAPbI$_3$ perovskite films, made on various underlayers.[40] The corresponding FWHM values of the reference- and NH$_2$-BA-based perovskites show the same value of 0.184, which may be ascribed to the pinhole formation as shown in Figure 1 a. Then, the FWHM reaches the lowest value of 0.137 for the Br-BA-based perovskite. The decreased value indicates decreased vacancies and proves the enhanced crystallinity, which is consistent with the bottom morphology images of Figure 1 a.

The WF of R-BA-modified NiO$_x$ NPs films were characterized by the ultraviolet photoelectron spectroscopy (UPS). As shown in Figure 2 a, the WF of the reference is 5.21 eV. If we use SAMs with negative dipole moment, say NH$_2$-BA, CH$_3$O-BA, and H-BA, to modify the surface of NiO$_x$ NPs, the WF calculated from the secondary cutoff will decrease to 4.82, 4.96, and 5.06 eV, respectively. However, for the NiO$_x$ NPs films modified by Cl-BA and Br-BA, which have a positive dipole moment, the WF respectively increases to 5.36 and 5.4 eV, which is aligned with the valence band maximum of MAPbI$_3$. This implies that a SAM with positive dipole moment can increase the WF of NiO$_x$ NPs films.

To investigate the effect of the R-BA modification on the device performance, we fabricated PSCs based on the following device structure, also shown in Figure S5: indium-doped tin oxide (ITO)/NiO$_x$ (with or without SAM)/MAPbI$_3$/PCBM/bis-C$_{60}$/Ag, where PCBM is [6,6]-phenyl-C$_{61}$-butyric acid methylester. As shown in Figure S6 and Table S1, the PCE of the PSCs based on the pristine NiO$_x$ film is 15.5% with a high V_{oc} of 1.07 V, which is similar to those obtained in previous work.[20] The NH$_2$-BA- and CH$_3$O-BA-modified devices show worse PECs, whereas the H-BA, Cl-BA, and Br-BA modification is found to enhance the device efficiency. The NH$_2$-BA-modified device has the lowest PCE, presumably owing to a large density of pinholes (see Figure 1 a) in the associated perovskite layer. In contrast, the Br-BA-modified device shows the highest PCE of 18.4%, with photovoltaic parameters enhanced compared with those of the reference device, that is, the V_{oc} increased from 1.07 to 1.11 V, J_{sc} increased from 19.6 to 21.7 mA cm^{-2}, and FF increased from 74.2 to 76.3%. This enhancement echoes the positive effect of the modification of NiO$_x$ film by Br-BA (c.f. the bottom images of Figure 1 a, b), which has led to the formation of pinhole-free, well-covered, and highly crystalline perovskite with suitable energy-level alignment. The enhanced UV/Vis absorption of the Br-BA-modified perovskite in Figure S7 also corroborates the improvement of J_{sc}.

We found that the V_{oc} decreases if a SAM modifier with negative dipole moment is applied, whereas the V_{oc} increases if the dipole moment is positive, which is well correlated with the WF change (ΔWF) of SAM-modified NiO$_x$ films. To investigate this observation, the variations of the V_{oc} and ΔWF versus
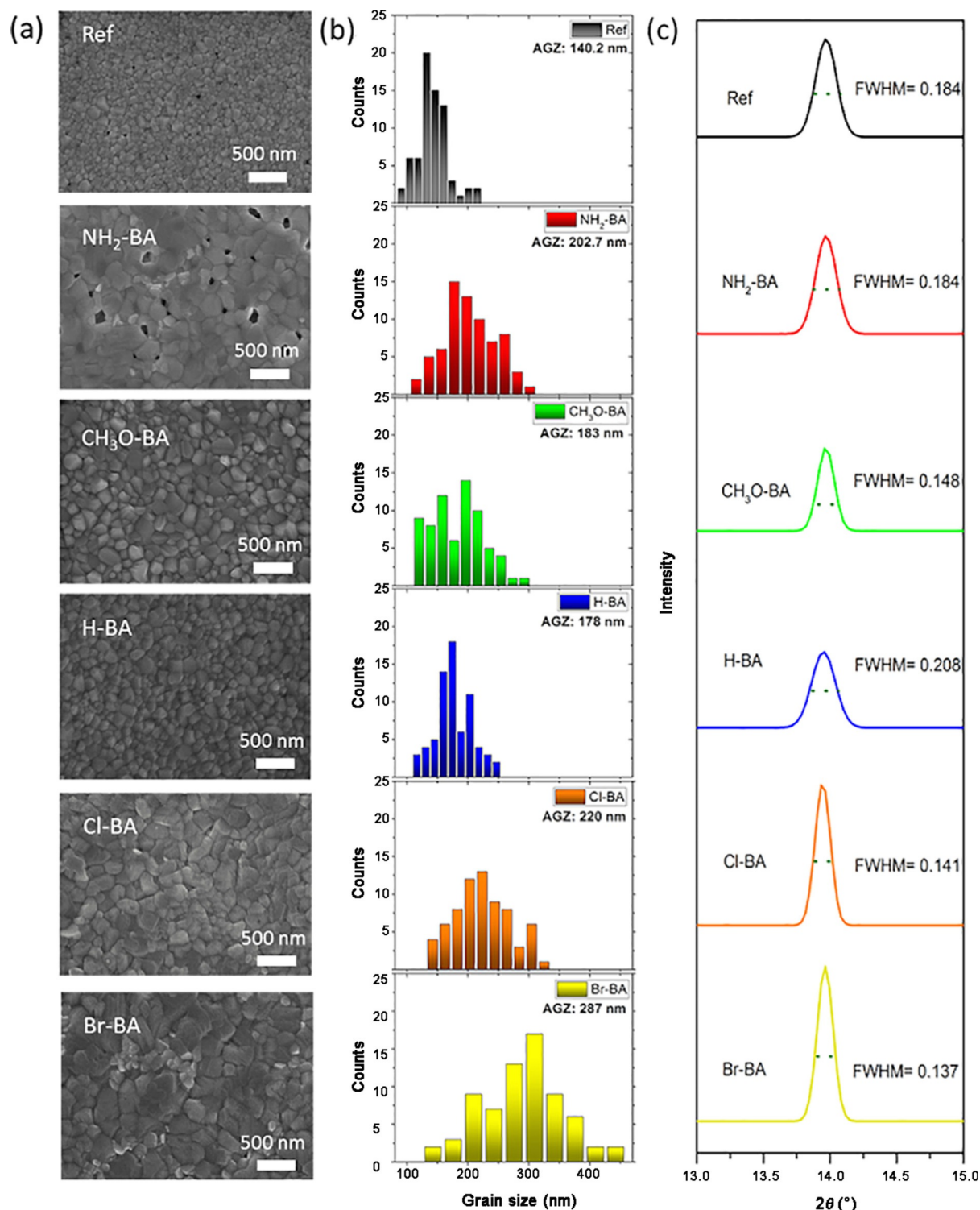
Figure 1. Morphology of a) the perovskite film deposited on various R-BA modified NiO$_x$ films; b) grain-size distribution of perovskite on various R-BA modified NiO$_x$ films; c) Gaussian distribution of the peak of the (110) plane and the FWHM value of perovskite film on the R-BA modified NiO$_x$ layer. Ref refers to reference group.

the dipole moment are shown in Figure 2b. Remarkably, the V_{oc} and ΔWF correlate well with the dipole magnitude through a linear relationship, which implies that the energy-level offset between the NiO$_x$ and perovskite could be fine-tuned by virtue of the dipole moments,[41] although the surface dipole concentration and the tilt angle between the dipole and the substrate

may also have certain influences.[39] In fact, the dipole could induce a step in the vacuum level under the effect of an electrical field. As illustrated in Figure 2c, the unmodified NiO$_x$ has an energy-level offset with the valence band maximum of the MAPbI$_3$ perovskite. After the interface modification by SAMs, the WF and the band edge will be changed and affect the V_{oc},
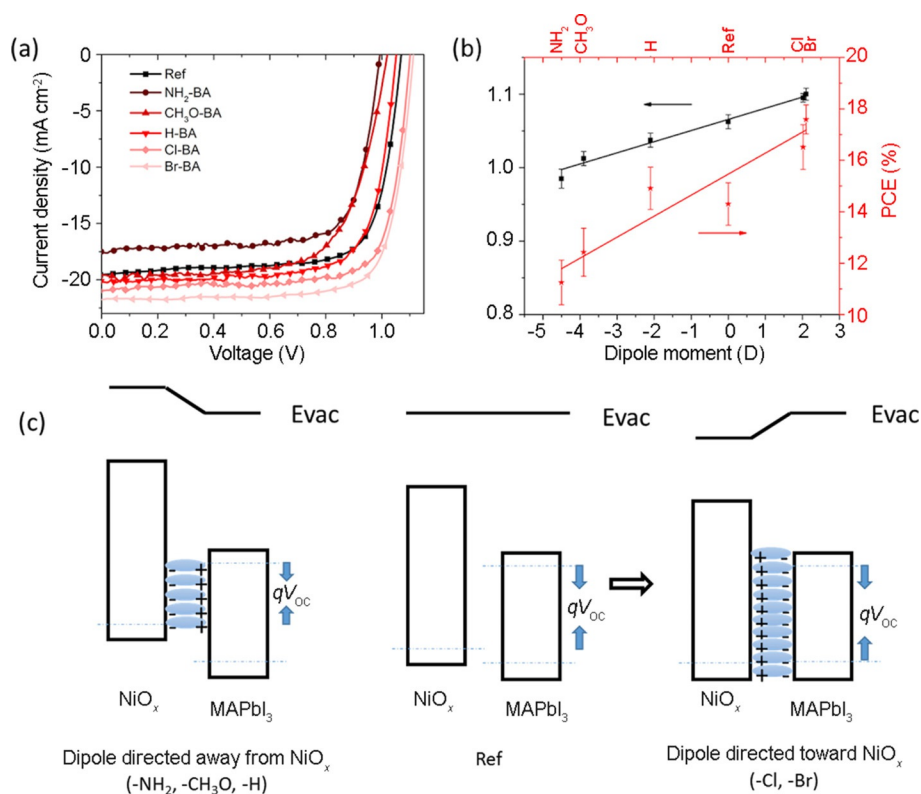
Figure 2. a) UPS curves of PSCs with or without various SAM modifications; b) V_{oc} and ΔWF plotted against the dipole moment of the SAMs; c) schematic diagram of the band bending caused by the SAMs with different dipole moments. Quasi-Fermi levels are shown as dashed lines.
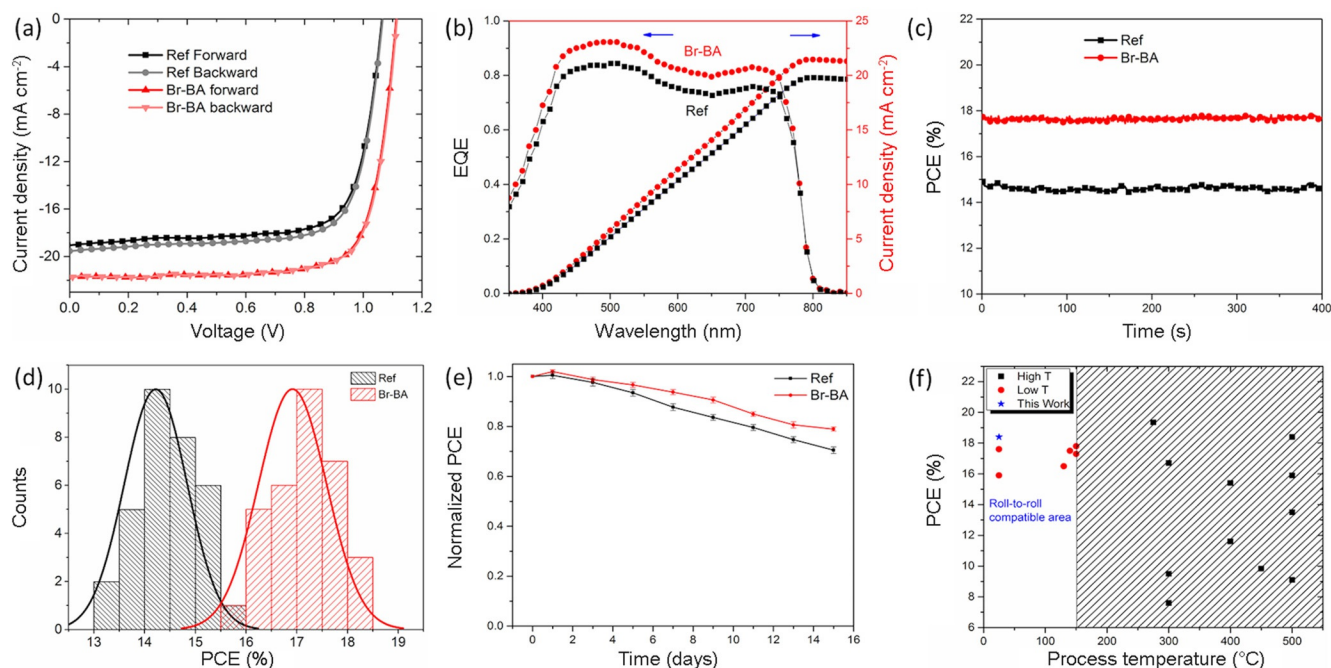
which is ideally determined by the effective band gap between the WF of NiO_x and the quasi-Fermi level of the conduction band in the $MAPbI_3$ perovskite. Additionally, if the surface dipole is pointed away from the NiO_x, the band edge will shift upward and the effective gap will reduce, that is, the V_{oc} decreases. However, if the surface dipole is pointed toward the NiO_x, the band edge will shift downward, increasing the effective gap and consequently the V_{oc} will increase. Our results are consistent with this band-bending theory.

To further investigate the merit of the SAMs modification, in Figure 3a and Table 1, we show the J–V curves and the photovoltaic parameters of the best-performing reference and the Br-BA-modified PSCs under both forward and reverse scan directions with a voltage sweeping rate of 0.1 V s^{-1}. For the reference device, there is subtle but obvious hysteresis resulting in a PCE of 15.3 % under the forward scan, and slightly different PCE of 15.5 % under the reverse scan. However, the Br-BA modification eliminates the hysteresis, showing a constant PCE value of 18.4 %, regardless of the scan direction. We further examined the scan rates of 0.01, 0.05, and 0.5 V s^{-1} and found that the PCEs of the Br-BA-modified devices show negligible hysteresis, which further corroborates the reliability of the Br-BA modification (c.f. Figure S8). The enhanced J_{sc} of the Br-BA-modified PSC may be attributed to the increased absorption and crystallinity of the perovskite layer, which is also confirmed by the corresponding external quantum efficiency (EQE) spectrum shown in Figure 3b. The improved FF value of the Br-BA-modified devices (c.f. Table 1) is speculated to be owed to effective pinhole passivation on the NiO_x NPs surfaces (c.f. Figure 2a) and the enhanced interfacial hole extraction,[42] resulting in an improved contact between the NiO_x and perovskite layers through the SAM linkages.

The steady-state output power has been proved as a more precise way to quantify the true PCE of solar cells.[43] By applying a bias around the maximum output power (0.89 V for the reference device, and 0.93 V for the Br-BA-based device), under AM1.5G illumination the steady-state PCE of the studied devices were recorded as 14.6 and 17.8 %, respectively, as shown in Figure 3c, which clearly verifies the device performance enhancement by the Br-BA modification. The histograms of the PCE of 32 fabricated devices with and without Br-BA modification are shown in Figure 3d. We can observe that the average PCE of the reference devices shows a PCE of 14.5 %, whereas that of the Br-BA-modified devices leaps to 17 % with a normal distribution, substantiating good reproducibility and reliability of the modification technique.

Table 1. Photovoltaic parameters of reference and Br-BA-based PSCs.

Sample	V_{oc} [V]	J_{sc} [mA cm^{-2}]	FF [%]	PCE [%]
reference forward	1.07	19.1	74.8	15.3
reference backward	1.07	19.6	74.2	15.5
Br-BA forward	1.11	21.7	76.3	18.4
Br-BA backward	1.11	21.7	76.3	18.4

Figure 3. a) *J–V* curves of the reference (Ref) and the Br-BA-modified PSCs under forward and reverse scan at a scan rate of 0.1 V s⁻¹; b) EQE spectrum and cumulative J_{sc} of the Br-BA-modified champion device; c) steady-state output power of the PSCs with and without Br-BA modification; d) PCE distribution of the devices with and without Br-BA modification; e) stability of the PSCs with and without Br-BA modification over 15 days stored under humidity of $\approx 30\%$; f) PCE versus process temperature of the PSCs incorporating NiO$_x$ layer presented in this work and by others in similar works. The data from the work of other groups and corresponding references can be found in Table S2.

The device stability or the long-term lifetime is another crucial photovoltaic parameter, as it determines its suitability for commercialization.[44] We therefore traced the PCE of the reference and Br-BA-modified devices under humidity of around 30% for 15 days, as shown in Figure 3e. The reference device maintained 70% of its original PCE, whereas the Br-BA-modified device maintained about 80% of its original PCE. The enhancement may be attributed to the enhanced crystallinity of the perovskite layer and decreased defect states of the NiO$_x$ film; the former improves the stability of the perovskite lattice and the latter impedes the permeation of water and oxygen into the inner perovskite film.[45]

We also compared the PCE versus processing temperature made by other groups that focus on the application of the NiO$_x$ in PSCs (Figure 3 f and Table S2). Although a newly accepted work about cesium-doped NiO$_x$-based PSCs achieved a record efficiency of more than 19%, its high temperature process (275 °C) severely restricts its application in flexible device fabrication.[46] In terms of commercialization, all layers should be processed under 150 °C. Based on Figure 3 f, our work substantiates the importance of the employed low-temperature-processed Br-BA-modified NiO$_x$ films incorporated in PSCs.

To better understand and ascertain the influence of the Br-BA SAMs on the NiO$_x$ film defects and perovskite crystallization, we obtained photoluminescence (PL) spectra (Figure 4 a,b) to examine the photocarrier dynamics of the MAPbI$_3$ perovskite deposited atop the NiO$_x$ film.[47,48] The steady-state PL intensity of MAPbI$_3$ deposited on the NiO$_x$ film is significantly lower than that deposited on bare glass, indicating that NiO$_x$ could effectively transfer the charges. As we deposited the

Br-BA SAM between the NiO$_x$ and MAPbI$_3$ layers, the PL intensity is further reduced, suggesting its role in surface passivation of the NiO$_x$ film, in which the charge carrier could be more effectively transferred in the device. This phenomenon can also explain the enhanced J_{sc} in the Br-BA-modified PSCs. The time-resolved PL (TRPL) decay of the studied devices are shown in Figure 4 b, where the TRPL curves demonstrate an obvious biexponential decay behavior. The fast decay portion of the spectrum corresponds to the trap-states quenching or charge transfer, whereas the longer decay portion reflects the bimolecular recombination.[35,47] Compared with the MAPbI$_3$ on bare glass, the NiO$_x$ could effectively quench the PL due to its hole-transporting ability. It is observed that the PL quenching of the Br-BA-modified NiO$_x$ film is further enhanced. The Br-BA modification not only helps the formation of a more uniform crystalline perovskite film, which is an indicative of shorter PL lifetime compared with the perovskite formed on the pristine NiO$_x$ film, but also functions as the linking agent between the NiO$_x$ and perovskite layers. Based on the data shown in Figure 4 b, we believe that the better contact induced by the Br-BA SAMs contributes to electrical coupling in the interfacial layer, and therefore results in an improved J_{sc}, as discussed before.

To understand the recombination mechanism of the studied devices, the *J–V* curves of the pristine and Br-BA-modified devices were obtained under light intensities ranging from 1 to 100 mW cm⁻², as shown in Figure S9. The power law dependence of the J_{sc} on the light intensity ($J \approx I^\alpha$) is plotted in Figure 4 c. According to the previous reports, α will be equal to 0.75 if the device has a space-charge limit due to the imbalanced carriers, or it will be equal to 1 if there is no space-
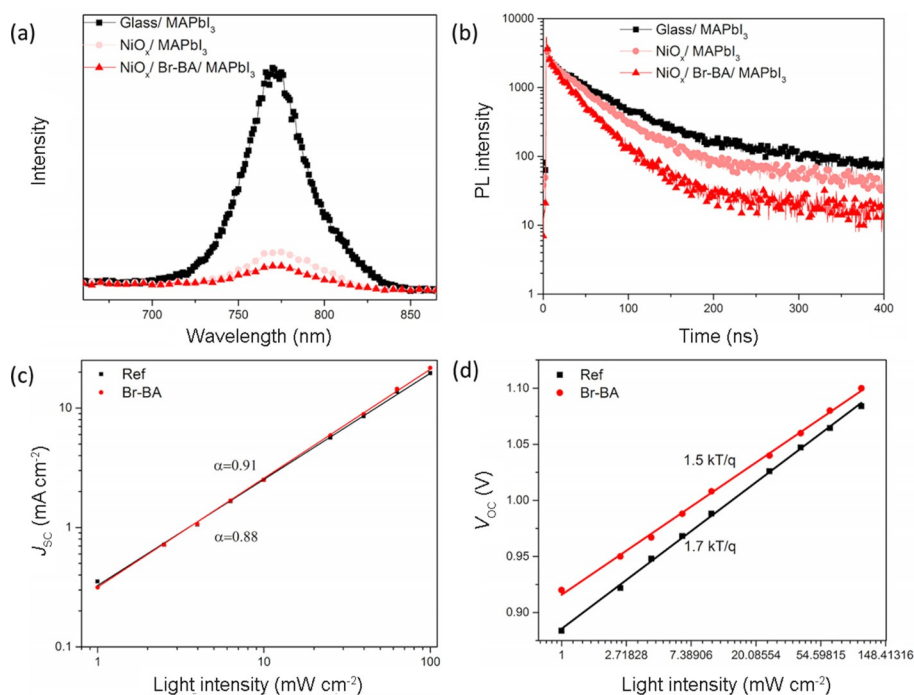
Figure 4. a) Steady-state PL and b) TRPL of the perovskite films made on bare glass, NiO_x, and Br-BA-modified NiO_x films; light intensity dependence of c) the J_{sc} and d) V_{oc} of the studied devices with and without Br-BA modification.

charge effects.[49] Here, for the pristine devices, α equals 0.88, whereas it equals 0.91 for the Br-BA-modified devices, indicating that the Br-BA-modified device is less affected by the space-charge limit. This suggests that the Br-BA modification could reduce the charge recombination and potential barriers, which could be envisaged as a result of defect passivation on the NiO_x surface.[50]

Because all photogenerated carriers will finally recombine at the open-circuit condition, investigating the relationship between the V_{oc} and light intensity is a rational method to precisely probe the trap-assisted recombination mechanism. By plotting the natural logarithmic relation between the V_{oc} and the light intensity in Figure 4d, we calculated the slope of the reference and Br-BA-modified devices, which are equal to $1.7\,kT/q$ and $1.5\,kT/q$, respectively, where k is the Boltzmann constant, q is the electron charge, and T is the temperature in Kelvin. It has been reported that a trap-free relationship would have a slope of $1\,kT/q$, whereas for the Shockley–Read–Hall recombination, the slope would be $2\,kT/q$.[51] Therefore, we can deduce that the Br-BA-modified devices have less trap-assisted recombination compared with the reference devices. Combined with the morphology diagrams in Figure 1a,b, we found that this reduced recombination results from the surface passivation of the NiO_x films and better crystallization of the perovskite layer, which collectively enhance the device photovoltaic performance.

As another major task, we then exploited the Br-BA SAM modification method on F-PSCs devices. The J–V curves depicted in Figure 5a show the photovoltaic performance of the champion devices of the Br-BA-modified PSC made on glass and the F-PSC made on the flexible PET substrate. As a major

consequence, the FF drops significantly from 76.3% on glass to 71.3% on PET, and the J_{sc} decreases to 20.7 mA cm^{-2}, but the V_{oc} maintains its value (1.10 V for PET versus 1.11 V for glass). This trend is reasonable because the flexible PET substrate might deteriorate the effective contact between each layer and thus induce the low FF and J_{sc}.[20, 22, 52] Even though the F-PSCs show a relatively lower PCE compared with the devices made on glass, the PCE of the Br-BA-modified F-PSCs reaches 16.2%, which is one of the highest PCE values for the F-PSCs, demonstrating the merit of the Br-BA SAM modification technique. For reliability measurements, we analyzed the PCE histogram of the F-PSCs over 32 devices in Figure 5b and the average value is around 15%, substantiating its decent reproducibility. To investigate the flexibility influence on the device performance, we conducted mechanical bending test as shown in Figure 5c. The F-PSCs could retain 75% of its initial PCE even after 110 bending cycles, proving the decent mechanical stability. The inset picture in Figure 5c shows the flexibility of the fabricated F-PSCs.

We have summarized the recent works about NiO_x HTL-based F-PSCs with PCEs larger than 10% (see Table S3) and compared the PCE and V_{oc} values with this work in Figure 5d. It is observed that the F-PSC herein shows the highest performance compared with other NiO_x-based F-PSC. In addition, the V_{oc} of our Br-BA-modified F-PSCs is significantly higher than those reported by the others, which could be ascribed to the better interface between the NiO_x and the perovskite layers, owing to the insertion of the Br-BA SAM modifier.

An important figure-of-merit of the optoelectronic devices is their PPW ratio, as it could combine and demonstrate the overall outcome of the high PCE, flexibility, and light weight.
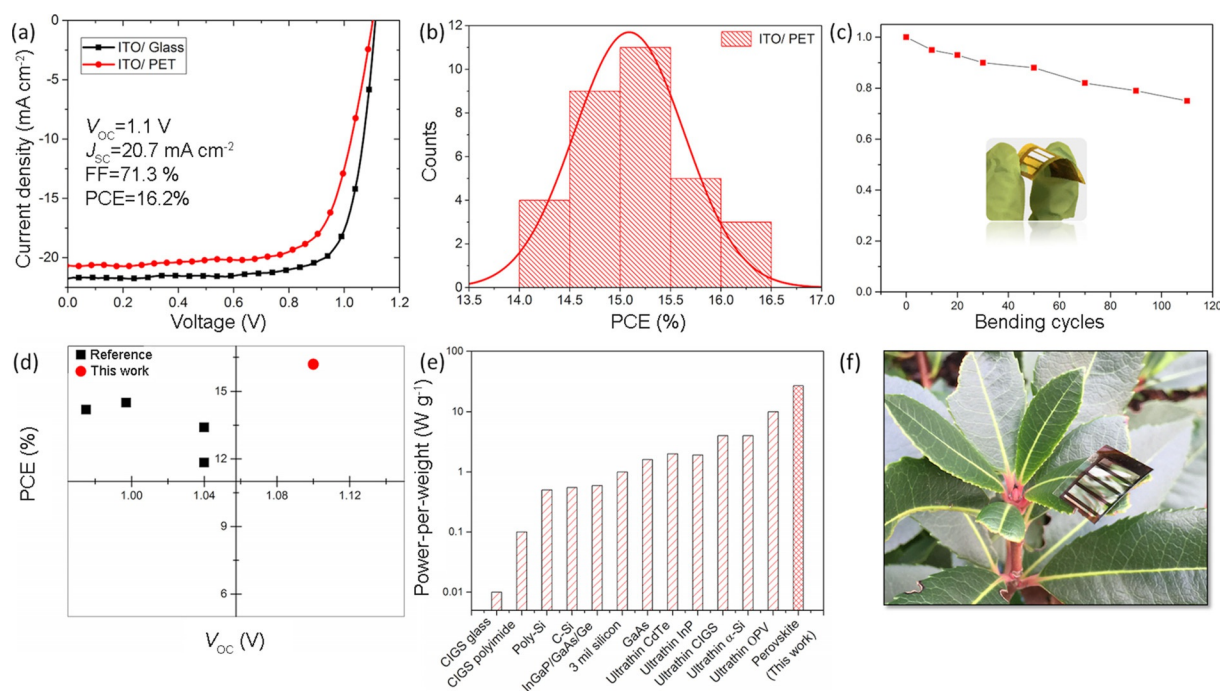
Figure 5. a) J–V curves of the Br–BA-modified PSCs made on glass substrates and F-PSCs made on flexible PET substrate; b) PCE distribution of the Br–BA modified F-PSCs over 32 devices; c) normalized PCE of the Br–BA modified F-PSCs as a function of the bending cycles (inset image shows a photograph of the F-PSC); d) comparison of the PCE and V_{oc} of the NiO$_x$-based F-PSCs shown in this work and by others; e) PPW comparison of various photovoltaic technologies (cell data are extracted from Ref. [52]); f) photograph of the fabricated ultralight SAM-modified F-PSC placed on a leaf.

Figure 5 e compares the typical PPW of the conventional crystalline silicon and inorganic and organic thin-film solar cells, showing that the F-PSC presented here outperforms all other solar cells and achieves a remarkable PPW of 26.9 W g^{-1} (see Table S4).[53] Figure 5 f shows our F-PSC placed on a green leaf, substantiating its light weight.

Conclusions

We developed a benzoic acid derivative self-assembled monolayer (SAM) interfacial modification method applied on low-temperature processed NiO$_x$ hole-transporting layer (HTL)-based inverted perovskite solar cells (PSCs). By using a series of SAMs with different dipole moments, we found that the SAM with positive dipole moments induces a band bending downward in the interface of the NiO$_x$ nanoparticles (NPs) and the perovskite layer, which could minimize the energy level offsets between the aforementioned layers, and consequently enhance the device V_{oc}. The best device performance was obtained through the Br-BA SAM modification by which the surface defects of the NiO$_x$ NPs were passivated and enhanced the perovskite crystallization. The collective positive effects of the SAM modification, including better energy-level alignment, better interfacial contact, surface passivation, and enhanced crystallization boosted the power conversion efficiency (PCE) of the studied devices to 18.4 %, with an open-circuit voltage (V_{oc}) of 1.11 V, short-circuit current (J_{sc}) of 21.7 mA cm^{-2}, and fill factor (FF) of 76.3 %, as well as enhanced stability, outperforming the reference device with an inferior PCE of 15.5 % and lower stability. Moreover, we applied the same SAM

modification method on a flexible PSC (F-PSC) and achieved one of the highest PCE of 16.2 % with a remarkable power-per-weight of 26.9 W g^{-1}. Our research shed light on the concept of interfacial engineering applied to low-temperature solution-processed metal oxide HTLs used in p-i-n PSCs, and the device performance results corroborated the great potential and promise of this technique for the development of commercially viable rigid or flexible PSCs.

Experimental Section

Materials: Methylammonium iodide (MAI) and bis-C$_{60}$ were home-made according to the procedure outlined in a previous work.[54] The NP-based NiO$_x$ thin films were synthesized according to the literature.[20] Other materials were purchased and used as received.

Solution preparation: NiO$_x$ NPs with a size distribution of about 5–10 nm were dispersed in water (20 mg mL^{-1}), and then ultrasonicated for 8 h; MAI (180 mg) and lead iodide (555 mg) were dissolved in a mixture (1 mL) of dimethyl sulfoxide (DMSO) and gamma-butyrolactone (GBL) solution (volume ratio of 3:7, respectively), and the resulting solution was stirred overnight. R-BA was dissolved in ethanol (2 mg mL^{-1}), and PCBM powder was dissolved in chloroform (CF) (15 mg mL^{-1}). Bis-C$_{60}$ was dispersed in isopropanol (IPA) and ultrasonicated for 3 h. All solutions were filtered before use.

Perovskite fabrication: ITO-coated glasses were first washed by detergent, deionized water, acetone, and IPA. Each washing process took 10 min. Then, ITO-coated glasses were treated in an UV–O$_3$ furnace for 15 min to increase the surface energy and make the

ITO surface more hydrophilic. For the flexible devices, PET substrate was used, as received. Then, the dispersion of NiO_x NPs in water was spun onto the ITO-coated glass or PET substrates at 3000 rpm for 30 s. R-BA solution was spun onto the NiO_x film at 2000 rpm for 30 s. The monolayer of the molecules was formed either through physical or chemical bonding between the R-BA and NiO_x NPs. The film was annealed on a hotplate at 90° for 5 min. To remove the physically absorbed molecules, ethanol was spun onto the film at 2000 rpm for 30 s several times. The R-BA-modified films were immediately transferred into a glovebox. Then, the perovskite solution was spun onto the SAM layer in two steps: first, the solution was spun at 1000 rpm for 15 s, and then the speed was immediately increased to 4000 rpm and spinning continued for another 45 s. During the last 25 s, toluene (800 µL) was dropped onto the spinning film in a continuous manner. Then, the substrate was placed on a hotplate at 100 °C for 10 min. After the sample was cooled to room temperature, the PCBM solution was spun over at 4000 rpm for 30 s, and then the bis-C_{60} solution was spun at 3000 rpm, for another 30 s. Finally, silver (120 nm) was thermally evaporated under high vacuum ($< 1 \times 10^{-6}$ torr, 1 torr $= 133.322$ Pa) to complete the device. The device area was measured with an aperture of 0.1 cm² to define the illumination area.

Characterization: The morphology of NiO_x and perovskite films was examined by an FEI Sirion XL30 SEM. The XRD data of the perovskite films were obtained using a Bruker F8 Focus Powder XRD machine. The UV/Vis absorption spectra of the perovskite films were recorded by a Varian Cary 5000 spectrophotometer. The UPS was performed under a discharged lamp with energy of 21.2 eV. The steady-state PL spectra were measured according to our previous study.[7] To obtain the TRPL spectra of the perovskite films with and without Br-BA modification, the films made on bare glass were first encapsulated by poly(methyl methacrylate) (PMMA), and then were placed under 510 nm laser head (LDH-P-C-510, PicoQuant, GmbH) pulsed at a repetition rate of 1 MHz, with a pulse duration of 117 ps. The J–V curves were measured using a 450 W xenon lamp solar simulator, using the AM1.5G filter, and a Keithley 2400 source meter. A KG3-filtered standard silicon photodiode detector was used to calibrate the light intensity before the measurements. The EQE spectra were obtained using an instrument equipped with a chopper with the frequency of 100 Hz, a Newport Cornerstone 130 monochromator, a standard Research Corp SR830 amplifier, a Keithley 2400 source meter, a silicon photodiode, which is certified by the National Institute of Standards and Technology (NIST) for calibration, and a xenon lamp (Oriel, 300 W). The stability measurements were conducted in a drybox filled with calcium oxide to control and maintain the relative humidity of 30 % at room temperature.

Conflict of interest

The authors declare no conflict of interest.

[1] M. A. Green, K. Emery, Y. Hishikawa, W. Warta, E. D. Dunlop, *Prog. Photovoltaics* **2016**, *24*, 905.

[2] J. H. Heo, S. H. Im, J. H. Noh, T. N. Mandal, C.-S. Lim, J. A. Chang, Y. H. Lee, H.-j. Kim, A. Sarkar, M. K. Nazeeruddin, M. Graetzel, S. I. Seok, *Nat. Photonics* **2013**, *7*, 486.

[3] N. J. Jeon, J. H. Noh, W. S. Yang, Y. C. Kim, S. Ryu, J. Seo, S. I. Seok, *Nature* **2015**, *517*, 476; V. W. Bergmann, S. A. Weber, F. J. Ramos, M. K. Nazeeruddin, M. Grätzel, D. Li, A. L. Domanski, I. Lieberwirth, S. Ahmad, R. Berger, *Nat. Commun.* **2014**, *5*, 5001.

[4] W. Yan, S. Ye, Y. Li, W. Sun, H. Rao, Z. Liu, Z. Bian, C. Huang, *Adv. Energy Mater.* **2016**, *6*, 1600474.

[5] Z. Bin, J. Li, L. Wang, L. Duan, *Energy Environ. Sci.* **2016**, *9*, 3424; Y. Wu, X. Yang, W. Chen, Y. Yue, M. Cai, F. Xie, E. Bi, A. Islam, L. Han, *Nat. Energy* **2016**, *1*, 16148.

[6] C.-C. Chueh, C.-Z. Li, A. K. Y. Jen, *Energy Environ. Sci.* **2015**, *8*, 1160.

[7] Q. Wang, C.-C. Chueh, M. Eslamian, A. K.-Y. Jen, *ACS Appl. Mater. Interfaces* **2016**, *8*, 32068.

[8] J. Kim, H. J. Park, C. P. Grigoropoulos, D. Lee, J. Jang, *Nanoscale* **2016**, *8*, 17608.

[9] Y. Bai, H. Chen, S. Xiao, Q. Xue, T. Zhang, Z. Zhu, Q. Li, C. Hu, Y. Yang, Z. Hu, F. Huang, K. S. Wong, H.-L. Yip, S. Yang, *Adv. Funct. Mater.* **2016**, *26*, 2950.

[10] J. H. Park, J. Seo, S. Park, S. S. Shin, Y. C. Kim, N. J. Jeon, H. W. Shin, T. K. Ahn, J. H. Noh, S. C. Yoon, C. S. Hwang, S. I. Seok, *Adv. Mater.* **2015**, *27*, 4013.

[11] F. Jiang, W. C. Choy, X. Li, D. Zhang, J. Cheng, *Adv. Mater.* **2015**, *27*, 2930.

[12] J. H. Kim, P. W. Liang, S. T. Williams, N. Cho, C. C. Chueh, M. S. Glaz, D. S. Ginger, A. K. Y. Jen, *Adv. Mater.* **2015**, *27*, 695.

[13] S. Liu, R. Liu, Y. Chen, S. Ho, J. H. Kim, F. So, *Chem. Mater.* **2014**, *26*, 4528.

[14] W. Chen, Y. Wu, Y. Yue, J. Liu, W. Zhang, X. Yang, H. Chen, E. Bi, I. Ashraful, M. Gratzel, L. Han, *Science* **2015**, *350*, 944.

[15] S. T. Williams, A. Rajagopal, C. C. Chueh, A. K. Jen, *J. Phys. Chem. Lett.* **2016**, *7*, 811.

[16] Z. Zhu, Y. Bai, T. Zhang, Z. Liu, X. Long, Z. Wei, Z. Wang, L. Zhang, J. Wang, F. Yan, S. Yang, *Angew. Chem. Int. Ed.* **2014**, *53*, 12571; *Angew. Chem.* **2014**, *126*, 12779; X. Yin, Z. Yao, Q. Luo, X. Dai, Y. Zhou, Y. Zhang, Y. Zhou, S. Luo, J. Li, N. Wang, *ACS Appl. Mater. Interfaces* **2017**, *9*, 2439.

[17] I. J. Park, G. Kang, M. A. Park, J. S. Kim, S. W. Seo, D. H. Kim, K. Zhu, T. Park, J. Y. Kim, *ChemSusChem* **2017**.

[18] F. C. Krebs, *Sol. Energy Mater. Sol. Cells* **2009**, *93*, 394.

[19] H. L. Zhu, J. Cheng, D. Zhang, C. Liang, C. J. Reckmeier, H. Huang, A. L. Rogach, W. C. Choy, *ACS Nano* **2016**, *10*, 6808.

[20] H. Zhang, J. Cheng, F. Lin, H. He, J. Mao, K. S. Wong, A. K. Jen, W. C. Choy, *ACS Nano* **2016**, *10*, 1503.

[21] X. Yin, J. Liu, J. Ma, C. Zhang, P. Chen, M. Que, Y. Yang, W. Que, C. Niu, J. Shao, *J. Power Sources* **2016**, *329*, 398; U. Kwon, B.-G. Kim, D. C. Nguyen, J.-H. Park, N. Y. Ha, S.-J. Kim, S. H. Ko, S. Lee, D. Lee, H. J. Park, *Sci. Rep.* **2016**, *6*, 35994.

[22] X. Yin, P. Chen, M. Que, Y. Xing, W. Que, C. Niu, J. Shao, *ACS Nano* **2016**, *10*, 3630.

[23] Y. Hou, W. Chen, D. Baran, T. Stubhan, N. A. Luechinger, B. Hartmeier, M. Richter, J. Min, S. Chen, C. O. Quiroz, N. Li, H. Zhang, T. Heumueller, G. J. Matt, A. Osvet, K. Forberich, Z. G. Zhang, Y. Li, B. Winter, P. Schweizer, E. Spiecker, C. J. Brabec, *Adv. Mater.* **2016**, *28*, 5112.

[24] W. C. Choy, D. Zhang, *Small* **2016**, *12*, 416.

[25] H. Ma, H. L. Yip, F. Huang, A. K. Y. Jen, *Adv. Funct. Mater.* **2010**, *20*, 1371.

[26] S. A. Paniagua, A. J. Giordano, O. L. Smith, S. Barlow, H. Li, N. R. Armstrong, J. E. Pemberton, J. L. Bredas, D. Ginger, S. R. Marder, *Chem. Rev.* **2016**, *116*, 7117.

[27] H.-L. Yip, S. K. Hau, N. S. Baek, H. Ma, A. K. Y. Jen, *Adv. Mater.* **2008**, *20*, 2376.

[28] X. Li, M. I. Dar, C. Yi, J. Luo, M. Tschumi, S. M. Zakeeruddin, M. K. Nazeeruddin, H. Han, M. Grätzel, *Nat. Chem.* **2015**, *7*, 703.

[29] P. E. Laibinis, G. M. Whitesides, *J. Am. Chem. Soc.* **1992**, *114*, 1990.

[30] J. Haruyama, K. Sodeyama, L. Han, Y. Tateyama, *J. Phys. Chem. Lett.* **2014**, *5*, 2903.

[31] C. Bi, Q. Wang, Y. Shao, Y. Yuan, Z. Xiao, J. Huang, *Nat. Commun.* **2015**, *6*, 7747.

[32] A. Abrusci, S. D. Stranks, P. Docampo, H. L. Yip, A. K. Jen, H. J. Snaith, *Nano Lett.* **2013**, *13*, 3124.

[33] L. Liu, A. Mei, T. Liu, P. Jiang, Y. Sheng, L. Zhang, H. Han, *J. Am. Chem. Soc.* **2015**, *137*, 1790.

[34] L. Zuo, Z. Gu, T. Ye, W. Fu, G. Wu, H. Li, H. Chen, *J. Am. Chem. Soc.* **2015**, *137*, 2674.

[35] L. Zuo, Q. Chen, N. De Marco, Y.-T. Hsieh, H. Chen, P. Sun, S.-Y. Chang, H. Zhao, S. Dong, Y. Yang, *Nano Lett.* **2017**, *17*, 269.

[36] H. Boehm, *Discuss. Faraday Soc.* **1971**, *52*, 264.

[37] S. K. Hau, H.-L. Yip, O. Acton, N. S. Baek, H. Ma, A. K. Y. Jen, *J. Mater. Chem.* **2008**, *18*, 5113.

[38] M. Bruening, E. Moons, D. Cahen, A. Shanzer, *J. Phys. Chem.* **1995**, *99*, 8368.

[39] C. Goh, S. R. Scully, M. D. McGehee, *J. Appl. Phys.* **2007**, *101*, 114503.

[40] N. Li, Z. Zhu, C.-C. Chueh, H. Liu, B. Peng, A. Petrone, X. Li, L. Wang, A. K. Y. Jen, *Adv. Energy Mater.* **2016**, *7*, 1601307.

[41] S. Rühle, M. Greenshtein, S.-G. Chen, A. Merson, H. Pizem, C. S. Sukenik, D. Cahen, A. Zaban, *J. Phys. Chem. B* **2005**, *109*, 18907.

[42] S. Chen, S. Yang, H. Sun, L. Zhang, J. Peng, Z. Liang, Z.-S. Wang, *J. Power Sources* **2017**, *353*, 123; M. Cha, P. Da, J. Wang, W. Wang, Z. Chen, F. Xiu, G. Zheng, Z.-S. Wang, *J. Am. Chem. Soc.* **2016**, *138*, 8581.

[43] H. J. Snaith, A. Abate, J. M. Ball, G. E. Eperon, T. Leijtens, N. K. Noel, S. D. Stranks, J. T.-W. Wang, K. Wojciechowski, W. Zhang, *J. Phys. Chem. Lett.* **2014**, *5*, 1511.

[44] G. Niu, X. Guo, L. Wang, *J. Mater. Chem. A* **2015**, *3*, 8970.

[45] J. M. Ball, A. Petrozza, *Nat. Energy* **2016**, *1*, 16149.

[46] W. Chen, F. Z. Liu, X. Y. Feng, A. B. Djurišić, W. K. Chan, Z. B. He, *Adv. Energy Mater.* **2017**, DOI: 10.1002/aenm.201700722.

[47] Q. Chen, H. Zhou, T. B. Song, S. Luo, Z. Hong, H. S. Duan, L. Dou, Y. Liu, Y. Yang, *Nano Lett.* **2014**, *14*, 4158.

[48] S. D. Stranks, G. E. Eperon, G. Grancini, C. Menelaou, M. J. P. Alcocer, T. Leijtens, L. M. Herz, A. Petrozza, H. J. Snaith, *Science* **2013**, *342*, 341.

[49] V. Mihailetchi, J. Wildeman, P. Blom, *Phys. Rev. Lett.* **2005**, *94*, 126602; L. Koster, V. Mihailetchi, H. Xie, P. Blom, *Appl. Phys. Lett.* **2005**, *87*, 203502.

[50] D. Zhao, M. Sexton, H.-Y. Park, G. Baure, J. C. Nino, F. So, *Adv. Energy Mater.* **2015**, *5*, 1401855.

[51] M. Mandoc, F. Kooistra, J. Hummelen, B. De Boer, P. Blom, *Appl. Phys. Lett.* **2007**, *91*, 263505; R. N. Hall, *Phys. Rev.* **1952**, *87*, 387.

[52] M. Kaltenbrunner, G. Adam, E. D. Głowacki, M. Drack, R. Schwödiauer, L. Leonat, D. H. Apaydin, H. Groiss, M. C. Scharber, M. S. White, *Nat. Mater.* **2015**, *14*, 1032.

[53] H. Zhang, J. Cheng, D. Li, F. Lin, J. Mao, C. Liang, A. K. Y. Jen, M. Grätzel, W. C. Choy, *Adv. Mater.* **2017**, *29*, 1604695.

[54] P. W. Liang, C. Y. Liao, C. C. Chueh, F. Zuo, S. T. Williams, X. K. Xin, J. Lin, A. K. Jen, *Adv. Mater.* **2014**, *26*, 3748; C.-Z. Li, C.-C. Chueh, H.-L. Yip, K. M. O'Malley, W.-C. Chen, A. K. Y. Jen, *J. Mater. Chem.* **2012**, *22*, 8574.